JOURNAL OF MATERIALS SCIENCE 18 (1983) 721–731

Viscoelastic characterization of poly(butylene terephthalate) using longitudinal resonances

R. K. GALKIEWICZ,* F. E. KARASZ
Materials Research Laboratory, Department of Polymer Science and Engineering, University of Massachusetts, Amherst, Massachusetts 01003, USA

The viscoelastic constants of poly(butylene terephthalate) were determined as a function of temperature using the harmonic dispersion of longitudinal resonances. Measured quantities were Young's modulus, Poisson's ratio and the logarithmic decrement, from which the bulk and shear moduli were derived. It was found that a dispersion relation used by Schwarzl and Struik can be employed to compensate for frequency dispersion of the modulus using no adjustable parameters. Measured quantities agree well with previously published values. Appendices are included which derive the resonant frequency shift due to damping in our specific experiment and which estimate the error introduced by the Schwarzl–Struik dispersion relation.

1. Introduction

Many methods [1] exist for determing the viscoelastic response of polymeric materials subjected to dynamic stresses. The majority of experimental techniques measure either one of the four dependent elastic constants, or one of these constants together with a quantity representing the internal loss in the sample (i.e. logarithmic decrement, $\tan \delta$, attenuation coefficient).

Owing to the difficulty in the direct measurement of Poisson's ratio, values have typically been obtained by calculation from Young's modulus and either the shear or bulk modulus. There is a difficulty, however, in using indirect methods, in that incompatabilities in the measured elastic constants – due to differing samples, sample thermal histories, measurement frequencies, strain levels, and anisotropy – can render derived constants unreliable. If Young's and shear moduli are used to derive Poisson's ratio, it can easily be shown that small uncertainties in these moduli can lead to relatively large uncertainties in the value obtained. Thus the ability to measure this quantity both directly (from a single set of measurements on a given sample) and simultaneously with another constant, presents a valuable experimental advantage.

In all resonance experiments one obtains an elastic modulus and a damping constant. If longitudinal resonances are employed, however, it is also possible to measure Poisson's ratio by examining the frequency dispersion from a pure harmonic sequence of resonance overtones. While this technique has been reported in the literature previously [2, 3], to our knowledge there have been no reports of the measurement of the dependence of Poisson's ratio determined by this method or of an attempt at a total viscoelastic characterization at one temperature for polymers or any other material.

In a previous publication [4] we have shown that the harmonic dispersion technique can be applied in a straightforward manner to low-loss materials over a wide temperature range. The purpose of this paper is to show that with some modification the technique can be used with materials which exhibit substantial relaxation mechanisms in the temperature–frequency region of interest.

2. Theory

In the lowest order approximation [5] the phase velocity, C, of longitudinal vibrations in a rod is given by $C = (E/\rho)^{1/2}$. Here E represents Young's

*Present address: 3M Center, St Paul, Minnesota, USA.

0022–2461/83/030721–11$03.82/0

modulus and ρ the density of the rod. If a sinusoidal stress is applied to the face of a rod of finite length L, then maximum displacement amplitude (resonance) is obtained at the end faces for discrete values of the wavelength, λ, given by $\lambda_n = 2L/n$ ($n = 1, 2, 3, \ldots$). The resonance frequencies, f, are thus given by

$$f_n = n(E/\rho)^{1/2}/2L, \tag{1}$$

and represent a pure harmonic series. (If, in actual practice, the rod is clamped midway along its length, the clamp defines a displacement mode and one examines only the odd harmonics: $n = 1, 3, 5, 7, \ldots$.) If end face displacement amplitude is monitored while the frequency is swept through a resonance peak then the logarithmic decrement is given by [6]

$$\Lambda_n = \pi \Delta f_n/f_n = \pi \tan \delta_n \tag{2}$$

where Δf_n is the peak width at half the maximum signal amplitude. It should be noted, however, that Equation 2 does not hold for arbitrarily large n; this will be discussed shortly.

A higher order elastic approximation for the phase velocity in a circular geometry is

$$C = \left(\frac{E}{\rho}\right)^{1/2}\left[1 - \left(\frac{\pi\nu r}{\lambda_n}\right)^2\right], \tag{3}$$

where ν represents Poisson's ratio and r the radius of the rod.

The correction term is due to the expansion and contraction of the rod circumference as a pressure wave travels along the sample; this gives rise to transverse (shear) as well as to longitudinal (elongation) displacements within the rod. For the values of r and λ_n employed in this work, the ratio of transverse to longitudinal displacements is quite small; however as r/λ_n increases, the ratio becomes large enough to (i) require the use of higher order terms in Equation 3, and (ii) bring into question the assumption underlying Equation 2 (i.e. does an appreciable shear damping component enter Λ_n with increasing transverse vibration?). For these reasons, values of r/L and n must be constrained so that the correction term amounts to $\lesssim 1\%$.

The normalized frequencies can be obtained from Equation 3:

$$\frac{f_n}{n} = \left(\frac{E}{\rho}\right)^{1/2}\frac{1}{2L}\left[1 - \left(\frac{\pi\nu r n}{2L}\right)^2\right] \tag{4}$$

so that a plot of f_n/n against the square of the harmonic mode number describes a straight line whose intercept and slope yield Young's modulus and Poisson's ratio, respectively. From these two elastic constants (E, ν) the shear and bulk moduli (G and K, respectively) can be calculated using

$$K = E/3(1 - 2\nu) \tag{5a}$$

and

$$G = E/2(1 + \nu). \tag{5b}$$

All four elastic constants (E, G, K, and ν) and a measure of the internal damping (Λ or $\tan \delta$) are thus obtained from one experiment consisting of the measurement of the odd-numbered longitudinal harmonic resonances of the sample.

In a low-loss material such as an inorganic glass well below its melting temperature, the above analysis carries over without modification [4]. For lossy materials – such as organic polymers which exhibit relaxation phenomena at or near the frequencies and temperatures of interest – the existence of a relaxation peak in Λ implies a frequency dispersion in E. This gives rise to two complications. Firstly, E can no longer be referred to as Young's modulus but must be specified as being either the absolute, storage, or loss modulus, denoted by $|E^*|$, E' and E'', respectively, where

$$E^* = E' + iE'' \tag{6}$$

and $i = \sqrt{-1}$. If Equation 1 is solved for E, one obtains for $n = 1$

$$E = 4\rho L^2 f_1^2. \tag{7}$$

If, on the other hand, a calculation similar to that of Horio and Onogi [9] (see Appendix 1) is performed for the system, then one finds that

$$E'(f_r) = 4\rho L^2 f_r^2\,[1 + \tfrac{1}{4}\tan^2 \delta\,(f_r)], \tag{8}$$

where f_r is the *measured* resonant frequency and $\tan \delta(f_r)$ is the *measured* loss at f_r. Therefore, it follows that (i) all moduli mentioned in this paper refer to the respective storage moduli unless otherwise explicitly noted, and (ii) data analysis proceeds as for the elastic case with f_n being replaced by $f_n[1 + (1/8)\tan^2 \delta(f_n)]$. Except in the region of maximum dispersion in $\tan \delta$ this correction is a negligibly small one.

Secondly, since one now finds that $E' \equiv E'(f)$, Equation 4 will in general no longer yield a straight line. In fact, to obtain the true value of ν, the dispersion contribution due to relaxation (as

distinct from geometry) must be subtracted from each harmonic overtone examined. This process can be performed at each temperature in the following manner.

(1) Harmonic overtones $n = 1, 3, 5, 7, 9, 11$ are determined, yielding values of f_n and $\tan \delta_n$.

(2) The modulus corresponding to f_3 is calculated from

$$E'(f_3) = \rho(2Lf_3/3)^2. \quad (9)$$

The third overtone is chosen because it is much less sensitive to various physical perturbing effects than is the first [4]. In fact, the fundamental is omitted throughout the remainder of the calculations. Also, there is no need to include a ν correction in Equation 9, as it will cancel out in Equation 11c, see below.

(3) The change in modulus due to frequency dispersion is then determined from the following relationship after Schwarzl and Struik [10] (see Appendix 2).

$$E'(f_{n'}) = E'(f_n)\left[\frac{1+\frac{1}{\pi}\ln(f_{n'}/f_n)\tan\delta(f_n)}{1-\frac{1}{\pi}\ln(f_{n'}/f_n)\tan\delta(f_{n'})}\right], \quad (10)$$

where n' is the next highest odd harmonic to n, i.e. $n' = n + 2$.

(4) At this point one has taken measured values of f_n, established a reference modulus E'_3, then calculated the dispersion due to relaxations of the modulus (a derived quantity) by utilizing the dispersion in $\tan \delta$ (a measured quantity). It is now necessary to translate this modulus dispersion back into frequencies. This is done by realizing that, similar to Equation 9,

$$(f_n)_{\text{observed}} = (n/2L)(E'_n/\rho)^{1/2}. \quad (11a)$$

However, what is desired is the adjusted value of f_n corresponding to E'_3, the reference modulus:

$$(f_n)_{\text{adjusted}} = (n/2L)(E'_3/\rho)^{1/2}. \quad (11b)$$

Dividing Equation 11b by Equation 11a and rearranging leads to:

$$(f_n)_{\text{adjusted}} = (f_n)_{\text{observed}}(E'_3/E'_n)^{1/2}. \quad (11c)$$

These adjusted frequencies (obtained using no additional parameters) are then employed in the plot of f_n/n against n^2 to determine both $E'(f_3, T)$ and $\nu(T)$.

Appendix 2 discusses the errors and assumptions involved in this calculation in detail.

3. Experimental details

3.1. Sample

The particular sample studied was cut from a section of 1.5 in. diameter rod of poly(butylene terephthalate) obtained from the Tennessee Eastman Company. Through careful machining, the sample was reduced to a rod of diameter 0.614 ± 0.007 cm and length 19.573 ± 0.003 cm. This rod was then placed in a cylindrical bore, heated under slight pressure to 221° C to relieve thermal stresses and cooled to room temperature at approximately 1° C min^{-1}. Aluminium electrodes were evaporated on to the lapped end faces of the rod and 0.009 cm diameter copper wire was attached to the side of the rod at each electrode using silver paint for grounding purposes. The mass of the sample was 7.7707 g yielding a density of 1.340 ± 0.001 g cm^{-3} at 23° C equivalent to a crystallinity of about 0.53.

3.2. Apparatus

A general description of the electronics has been given previously [4]. The sample support system was substantially modified as follows. The sample was supported at the centre by three dulled razor blades spaced equidistant around the circumference. While two of these edges were clamped firmly in place, the third was spring-loaded so as to keep constant tension on the sample independent of temperature and the thermal expansion differential between the sample and sample holder. This differential also necessitated the construction of adjustable transducer mounts. The final design is shown in Fig. 1 in which the sample, sample holder, and transducers are set into a copper tube of approximate length 28 cm and inner diameter 2.5 cm. Nichrome wire enclosed in teflon tubing was wrapped around the copper tube in two independent coils as indicated. Two copper–constantan thermocouple junctions were then placed into the tube to measure thermal gradients along the length of the tube. The assembly was placed inside a large copper can which was then evacuated and immersed in a constant temperature bath for sub-ambient measurements. For above-ambient temperatures, a heating tape was wrapped about the outside of the can which was placed in a dry dewar and the entire can was heated with the tape and a proportional device (Versa-Therm, model 2156; Cole Parmer Instrument Co). Control rods were introduced through the can top to adjust the transducers to the data-taking

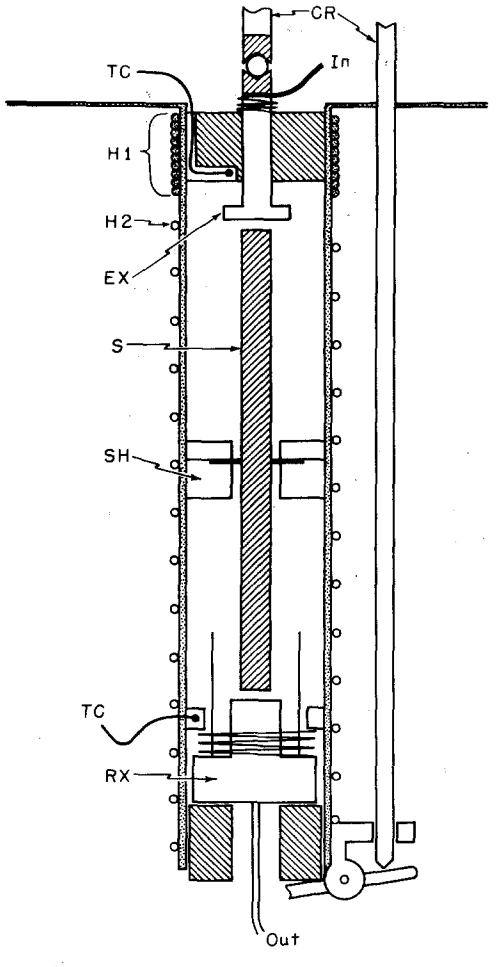

Figure 1 Schematic drawing of the sample holding/transducer apparatus. Shaded regions represent electrical insulators. For clarity, grounding wires are not shown and the sample–transducer gaps are exaggerated. CR = control rod; IN = signal input; TC = thermocouple; H1, H2 = nichrome heater coils; EX = excitation transducer; S = sample; SH = sample holder; RX = response transducer; Out = signal output.

position (approximately 0.001 cm from the sample ends).

The overall procedure was as follows: the vacuum can was evacuated and flushed with helium several times. The can was immersed in liquid nitrogen and, after equilibrium was established, the odd resonances up to $n = 11$ were measured and the $n = 1$ reasonance was repeated as a check for drift in temperature over the time required (roughly 1 h) to scan the seven resonances. The sample temperature was then raised, with care taken to keep the readings of both thermocouples as close as possible (generally within 0.3 K). Once the thermocouple readings were stabilized, roughly 1 h was allowed for the sample to reach thermal equilibrium; the resonances were than scanned with a repeat of the $n = 1$ resonance exactly as before.

A liquid nitrogen bath was employed from 77 to 199 K, followed by methanol/methanol ice (172 to 169 K), methanol/dry ice (205 to 282 K), and ice/water (273 to 292 K).

During the course of a run, a grounding wire separated from the sample necessitating a warming to ambient, re-evaporation of electrodes and grounding wire, remounting of the sample and a cooling to liquid nitrogen temperatures. It is significant to note that the change in the normalized resonant frequencies before and after the repair and remounting was less than 5 Hz and averaged approximately 2 Hz over all the resonances, i.e. one part in 3000. This error is of the order of the scatter in the data at those temperatures. Evidently, the reproducibility of the data is remarkably independent of sample mounting or loading due to the evaporated electrode, silver paint, and fine copper wire.

4. Results

Plotted in Figs. 2 and 3 are values of tan δ_n against temperature for poly(butylene terephthalate). As the temperature is increased, tan δ_n passes through a distinct maximum, decreases and then rises again sharply as the glass transition region is approached. As the mode numbers increase, the peak amplitudes increase and peak centres shift to higher temperatures; the values at the temperature extremes are frequency-independent. The scatter can be seen to increase with mode number; this effect is due primarily to a decreasing signal-to-noise ratio with increasing mode numbers [4].

Fig. 4 shows an Arrhenius plot of peak frequency as a function of inverse temperature which yields an activation energy of 10.7 kcal mol^{-1}, in good agreement with a value of approximately 9.7 kcal mol^{-1} obtained from a Rheovibron study by Nemoz *et al.* [11].

The low temperature relaxation shown in Figs. 2 to 4 has been observed in PBT by many authors. Farrow *et al.* [12] believed that the relaxation was a superposition of two peaks which shifted in relative strength and position as the number of methylene units was increased in the homologous series of poly(alkylene terephthalates). Illers and Breuer [13] concluded that the lower temperature relaxation was due to hindered

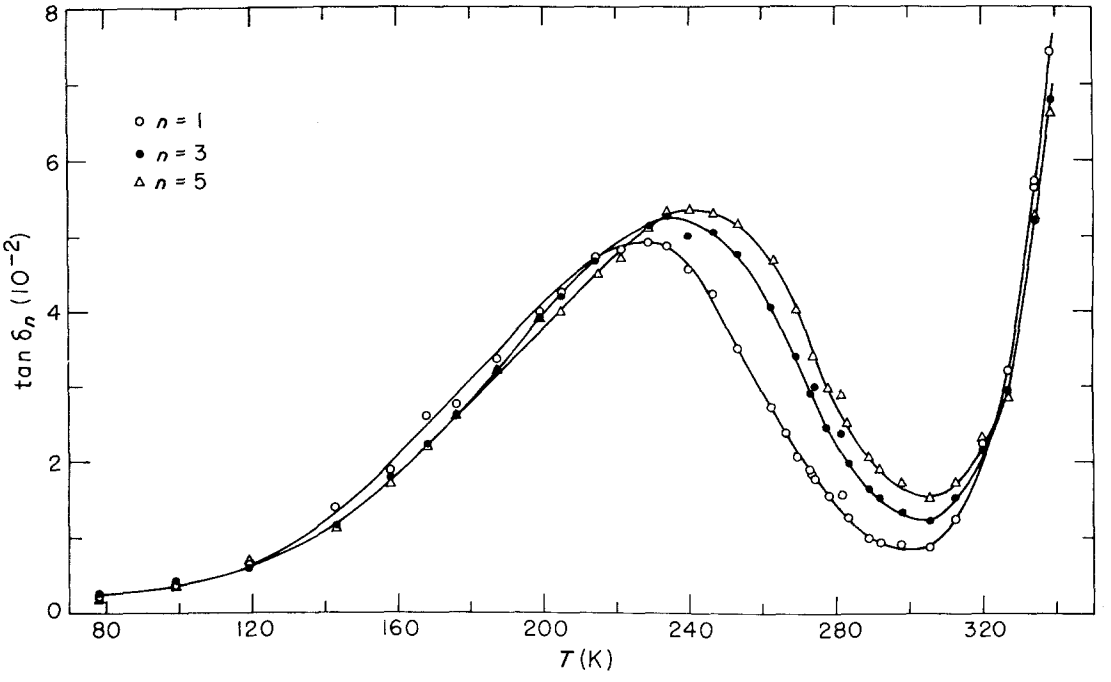

Figure 2 Plot of tan δ_n as a function of temperature for modes $n = 1, 3, 5$ for PBT.

rotation of methylene groups while that at the higher temperature was due to COO group movements. Later, Nemoz *et al.* [11] postulated that the two peaks superimposed were due to *trans* and *gauche* methylene movements in the amorphous phases.

Since the relative magnitude and location of the peaks varies within the frequency–temperature plane, the resultant experimentally-determined peak shows varying degrees of asymmetry. For PBT, Nemoz *et al.* [11] found the relaxation to be very symmetrical at 110 Hz with slight

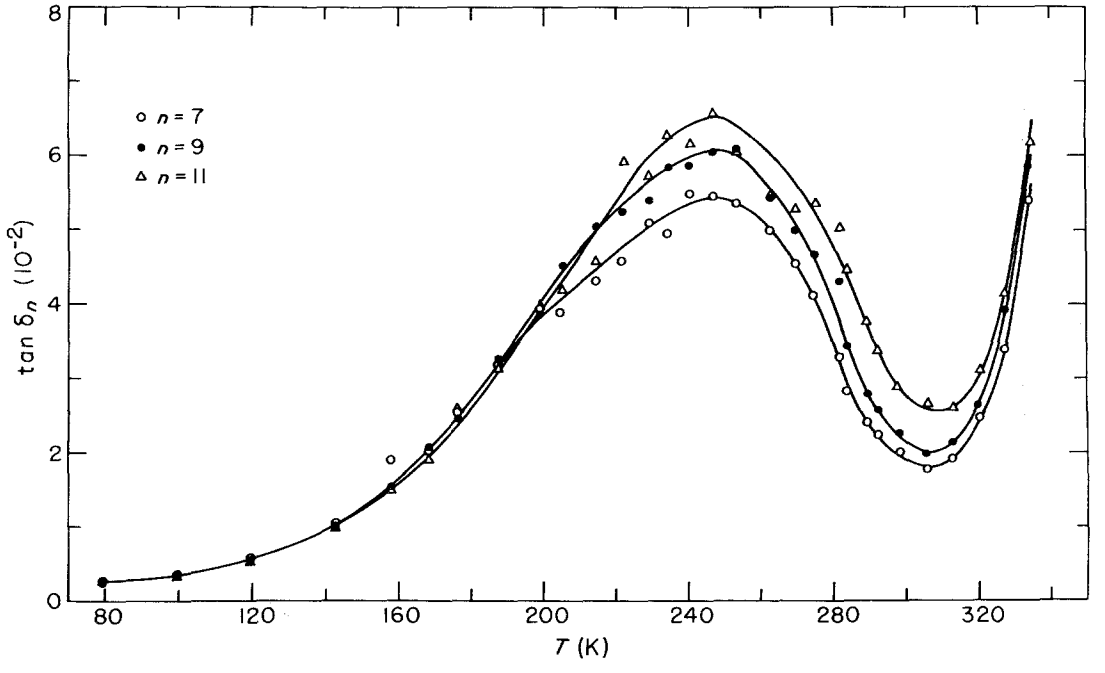

Figure 3 Plot of tan δ_n as a function of temperature for modes $n = 7, 9, 11$ for PBT.

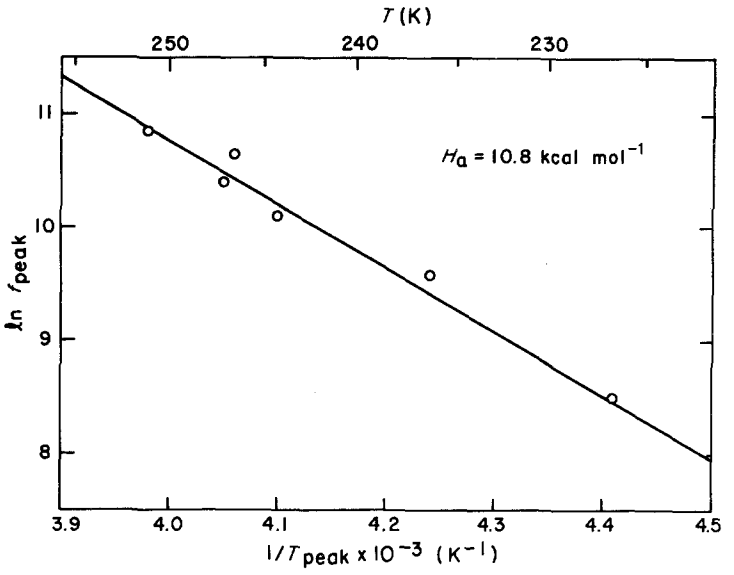

Figure 4 Plot of $\ln f_{peak}$ against $1/T_{peak}$ for the data presented in Figs. 2 and 3. The least squares fit yields an activation energy of 10.8 kcal mol^{-1}.

skewing towards higher temperatures (see Figs. 4 and 7 in Nemoz *et al.* [11]). Some slight asymmetry can also be seen in Figs. 2 and 3 with the curves skewed towards higher temperatures. This behaviour could possibly be enhanced by overlap with the glass transition relaxation, especially at the higher frequencies. It should be noted that in common with all resonance experiments the curves do not represent isochronous conditions. However, the correction in terms of peak shape are negligible.

Fig. 5 shows the dependence of the storage modulus on temperature, at a nominal frequency

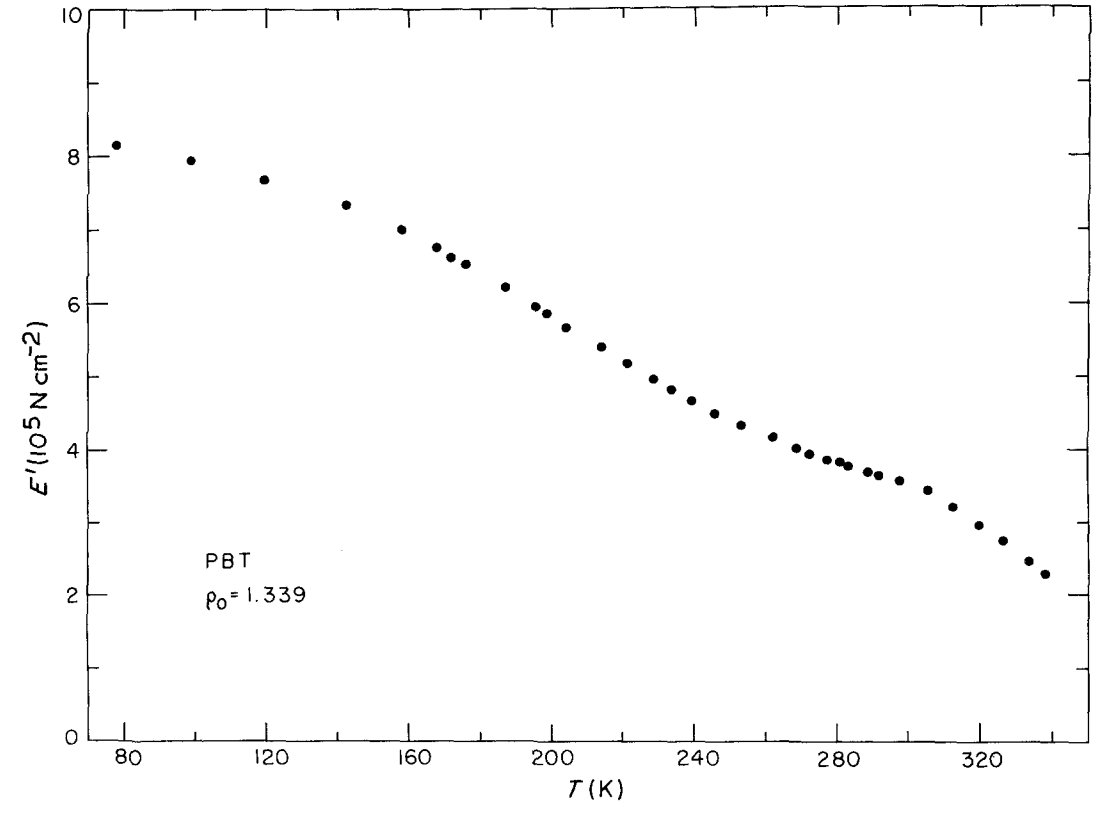

Figure 5 Storage modulus as a function of temperature for PBT.

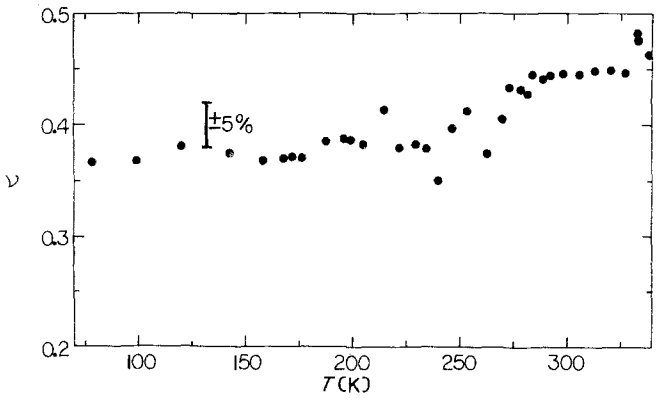

Figure 6 Poisson's ratio as a function of temperature for PBT.

of 15 kHz. An inflection point occurs at roughly 230 K which corresponds well to the maximum of $\tan \delta_1$ in Fig. 3 while the rapid decrease for $T > 300$ K is correlated with the sharp increase in $\tan \delta$ in the same temperature region, indicative of the approaching glass transition. The error bars are less than or of the order of the point size on the figure, as is the experimental scatter.

Fig. 6 shows Poisson's ratio as a function of temperature. A very slight increase is seen up to roughly 250 K followed by a sharper rise to a value near 0.45. The region of this rise also shows increased scatter which is probably due to the concommitant larger dispersion and scatter in $\tan \delta_n$ with frequency shown in Figs. 2 and 3. With the exception of four or five points the overall scatter in ν is very reasonable, amounting to about ± 3%.

The values of ν obtained in this work fall generally within the bounds of 0.38 measured by Takemori [14] and 0.44 determined by Warfield *et al.* [15]. These researchers employed far larger strain amplitudes and different frequency regimes to obtain their (ambient temperaure) values so that direct comparisons of data are questionable.

It should be noted that although this technique can provide four elastic constants together with the loss tangent for isotropic solids, the sensitivity to error in the bulk modulus, K, increases as ν approaches its maximum value of 0.5. This is shown in Fig. 7. The scatter in K renders estimation useless to $\lesssim 30\%$, while that in G is an order of magnitude smaller. The reason for this behaviour can be found by differentiating Equations 5a and b to obtain

$$dK/K = dE/E + 2d\nu/(1 - 2\nu) \quad (12a)$$

and

$$dG/G = dE/E + d\nu/(1 + \nu). \quad (12b)$$

Using values of $dE/E = 0.1\%$ and $d\nu/\nu = 5\%$, relative errors in K and G are obtained. While dG/G is less than 2% for all values of ν, dK/K is unbounded, reaching 100% at $\nu = 0.476$.

One may conclude then, that the technique employed in this work is very useful for determining E, ν, G, and $\tan \delta$. However, for most polymers $\nu \gtrsim 0.3$ so that derived values of K are susceptible to inaccuracy and scatter.

5. Conclusions

A method to unambiguously measure E, ν, and $\tan \delta$ in polymeric systems is proposed. From these viscoelastic constants one can calculate G and K although for $\nu \gtrsim 0.4$ the scatter in K is generally large. In particular the technique has substantial advantages for obtaining Poisson's ratio as a function of temperature at very low strain amplitude.

Results of employing this technique on poly(butylene terephthalate) are in good agreement with previous investigations although direct comparisons are not possible due to the utilization of different strain amplitudes and frequency regimes among the various experiments. We believe that some of the experimental scatter in Poisson's ratio can be reduced by better temperature regulation.

The technique is now being applied to polymer–glass isotropic composite systems where it will be used to study the effects of inclusions on mechanical properties as a function of wt% filler and temperature.

Acknowledgements

We would like to thank P. R. Couchman for helpful discussions. This research was supported by AFOSR 80-0101.

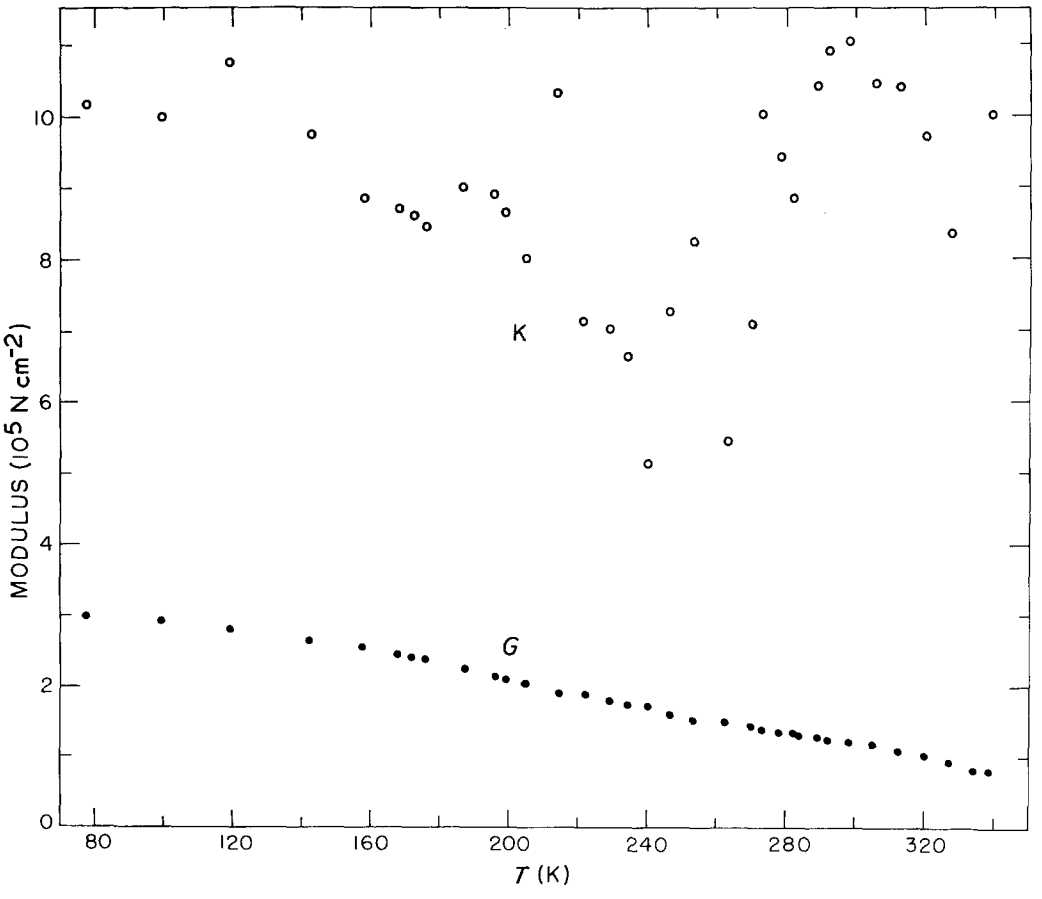

Figure 7 Derived values of bulk and shear moduli as a function of temperature for PBT. These values are calculated using Equation 5a, b and the data shown in Figs. 5 and 6.

Appendix 1

Consider a uniform rod of length, L, density, ρ, and cross-sectional area, A. At any point, x, along the length the stress can be related to the strain by

$$\sigma(x, T) = \frac{F(x, T)}{A} = \left(E' + \eta \frac{\partial}{\partial t}\right) \frac{\partial}{\partial x} u(x, t), \tag{A1}$$

where σ is stress, F is force and u is particle displacement at x and time t; E' represents a modulus of elasticity and η a coefficient of viscosity. If one assumes the usually separation of variables and time dependence in $\exp(i\omega t)$, Equation A1 becomes

$$\sigma(x) = (E' + i\omega\eta) \frac{\partial u(x)}{\partial x}. \tag{A2}$$

Defining a complex modulus by $E^* = E' + iE''$ and a phase angle by $\tan \delta = E''/E'$, we see that

$$E'' = \eta\omega \tag{A3a}$$

and

$$\tan \delta = \eta\omega/E'. \tag{A3b}$$

Establishing a force balance in the usual manner [5] but employing Equation A2, one obtains

$$\frac{\partial^2}{\partial x^2} u(x) + q^2 u(x) = 0 \tag{A4}$$

where

$$q^2 = \omega^2 \rho/(E' + i\omega\eta), \tag{A5}$$

and admits the general solution

$$u(x) = A_0 \cos qx + B_0 \sin qx. \tag{A6}$$

To reproduce the experimental procedure, we apply a force of constant amplitude, F_0, at $x = L$ and no force at $x = 0$, constraining the constants of integration to be given by

$$B_0 = 0 \tag{A7a}$$

$$A_0 = \frac{-F_0 q}{\omega^2 \rho A \sin qL}. \tag{A7b}$$

Letting $qL = \alpha + i\beta$ one can easily show that

$$\alpha^2 = (\omega^2\rho L^2/E')\left[\frac{(1+\tan^2\delta)^{1/2}+1}{2(1+\tan^2\delta)}\right] \quad \text{(A8a)}$$

$$\beta^2 = (\omega^2\rho L^2/E')\left[\frac{(1+\tan^2\delta)^{1/2}-1}{2(1+\tan^2\delta).}\right] \quad \text{(A8b)}$$

Experimentally, resonance is determined by measuring the square of the displacement amplitude at $x = 0$. This is given by

$$|u(0)|^2 = |A_0|^2 = \left(\frac{F_0}{AE'}\right)^2\left[\frac{1+\beta^2/\alpha^2}{(\sin^2\alpha+\sinh^2\beta)(1+\frac{3}{4}\tan^2\delta)}\right]. \quad \text{(A9)}$$

Now, for the pure elastic case, $\eta = 0$ and resonance occurs at $\omega = \omega_0$ so that

$$\alpha = \alpha_0 = (\omega_0^2\rho L^2/E') \quad \text{(A10a)}$$

$$\beta = 0 \quad \text{(A10b)}$$

and

$$|u(0)|^2 = (F_0/AE')^2/\sin^2\alpha_0. \quad \text{(A10c)}$$

The condition for maximization of Equation A10c is $\alpha_0 = \pi$ (and integer multiples) so that from Equation A10a we have

$$E' = \rho(L\omega_0/\pi)^2. \quad \text{(A11)}$$

For real materials $\eta > 0$ and the resonance frequency is shifted to

$$\omega_r = \omega_0 + \Delta\omega = \omega_0\left(1+\frac{\Delta\omega}{\omega_0}\right), \quad \text{(A12)}$$

that is, ω_r is the measured resonant frequency. The problem of relating E' to the measured resonance frequency thus reduces to that of finding $\Delta\omega/\omega_0$ in terms of η, or more conveniently, $\tan\delta$.

One can solve this problem either analytically or numerically. Analytically, the procedure [9] is to approximate α and β in the limit of small $\tan\delta$ and $\Delta\omega/\omega_0$, substitute into Equation (A9), take a partial derivative with respect to α, and set that expression equal to zero. A resonant value for α can then be found in terms of ω, η, and E' that can be related to ω_r to solve for $\Delta\omega/\omega_0$. An alternative method is to solve the problem numerically by specifying η/E' and varying ω about ω_0. This varies α and β, given *exactly* by Equation A8 as a function of ω and $\tan\delta$, and these functions are inserted into Equation A9. The quantity $|u(0)|^2$ is then maximized for a given value of frequency ω_r and $\tan\delta$ $(= \omega\eta/E')$. Values of $\Delta\omega/\omega_0$ are then obtained at different values of $\tan\delta$ and the results plotted. These results show that in the limit of small $\tan\delta$ we have

$$\frac{\Delta\omega}{\omega_0} = -\frac{1}{8}\tan^2\delta \quad \text{(A13)}$$

which then leads to Equation 8.

In addition to showing the general dependence, the calculations also show the deviation from Equation A13 with increasing $\tan\delta$. For instance at $\tan\delta = 0.06$, the maximum value for our data, Equation A13 underestimates the exact value by roughly 2%.

As a check of the computer calculations, an expression analogous to Equation A9 for the damped driven harmonic oscillation was tested and yielded

$$\frac{\Delta\omega}{\omega_0} = -\frac{1}{4}\tan^2\delta \quad \text{(A14)}$$

for small $\tan\delta$, good to 0.1% at $\tan\delta = 0.09$, in accord with theory (see, for example [16]).

Appendix 2

Following Schwarzl and Struik [10] we write

$$\frac{dE'(\omega)}{d\ln\omega} = \frac{2}{\pi}E''(\omega), \quad \text{(A15)}$$

where we have replaced the shear modulus by Young's modulus and $\omega = 2\pi f$. Upon integrating one obtains

$$E'(\omega_2) - E'(\omega_1) = \frac{2}{\pi}\int_{\ln\omega_1}^{\ln\omega_2} E''(\omega)\, d\ln\omega, \quad \text{(A16)}$$

and approximating the integration areas as a trapezoid we have

$$E'(\omega_2) = E'(\omega_1) + \frac{2}{\pi}\left[\frac{E''(\omega_2)+E''(\omega_1)}{2}\right]\ln\frac{\omega_2}{\omega_1}. \quad \text{(A17)}$$

Finally, letting $E''(\omega) = E'(\omega)\tan\delta\ (\omega)$ and rearranging we have

$$E'(\omega_2) = E'(\omega_1) \times \left[\frac{1+(1/\pi)\ln(\omega_2/\omega_1)\tan(\omega_1)}{1-(1/\pi)\ln(\omega_2/\omega_1)\tan(\omega_2)}\right], \quad \text{(A18)}$$

which is equivalent to Equation 10.

While no approximations exist in going from Equation A17 to A18, there are approximations involved in Equations A15 and A17. We can obtain a measure of the reliability of Equation A17 in the following manner.

Recall that $E'(\omega)$ and $E''(\omega)$ can be written in terms of the relaxation spectrum $H(\tau)$ as

$$E'(\omega) = \int_{-\infty}^{\infty} \mathrm{d} \ln \tau \, H(\tau) \frac{\omega^2\tau^2}{1+\omega^2\tau^2} + E_0 \tag{A19a}$$

and

$$E''(\omega) = \int_{-\infty}^{\infty} \mathrm{d} \ln \tau \, H(\tau) \frac{\omega\tau}{1+\omega^2\tau^2} . \tag{A19b}$$

Rewriting Equation A17 in terms of Equation A19a and b we obtain

$$\int_{-\infty}^{\infty} \mathrm{d} \ln \tau \, H(\tau) \frac{\omega_2^2\tau^2}{1+\omega_2^2\tau^2} = \int_{-\infty}^{\infty} \mathrm{d} \ln \tau \, H(\tau) F(\omega_2, \omega_1, \tau) \tag{A20}$$

where

$$F(\omega_2, \omega_1, \tau) = \frac{\omega_1^2\tau^2}{1+\omega_1^2\tau^2} + \frac{\ln(\omega_2/\omega_1)}{\pi} \left(\frac{\omega_2\tau}{1+\omega_2^2\tau^2} + \frac{\omega_1\tau}{1+\omega_1^2\tau^2} \right). \tag{A21}$$

Consequently, Equation A17 can be tested by performing the integration in Equation A20 over some reasonable interval, given a function $H(\tau)$.

We proceed by assigning

$$H(\tau) = H_0 \left[\frac{\tau/\tau_0}{1+(\tau/\tau_0)^2} \right]^m , \tag{A22}$$

which represents a logarithmically symmetric function peaked at $\tau = \tau_0$ whose half-width is given by $\Delta\tau = 2(2^{2/m} - 1)^{1/2}$. We then let $\omega_2/\omega_1 = 5/3$, representing an estimate of the fifth harmonic from the third, the longest and thus worst-case frequency estimate employed in the experiment. Finally, let $\omega_1 = R/\tau_0$ where $10^{-4} \leqslant R \leqslant 1$ (the region of maximum expected error for Equation A20) and integrate from $10^{-40} \leqslant \tau/\tau_0 \leqslant 10^{+40}$. In general the integrations must be performed numerically; however, for the special case $m = 0$ one can obtain an exact expression for the left integral as a check of the accuracy of the numerical method. For our conditions the agreement was found to be better than one part in 10^{+6}. For $m = 0.425$, representing a half-width of one decade, Equation A20 is in error less than 2% and for a more realistic half-width of two decades ($m = 0.177$) the accuracy is better than 0.5%. Of course these results are independent of H_0 and E_0.

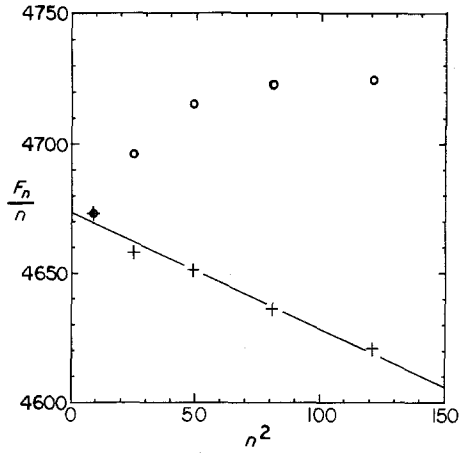

Figure A1 Normalized frequency as a function of mode number squared at 246.5 K for poly(butylene terephthalate). The circles represent raw data, and the crosses data corrected for damping and frequency dispersion.

To determine how well Equation A20 applies to the experimental data, H_0 and E_0 are determined by employing the known experimental values of E' and E'' at maximum damping. Because $\mathrm{d} \tan\delta\,(f)/\mathrm{d}f \leqslant 0$ at all temperatures (see Equations 2 and 3), $\omega_1\tau_0 = 1$ is never attained and at most $\omega_1\tau_0 = R \leqslant 3/11$. If Equation A20 is now examined with the derived values of E_0 and H_0, a 0.07% error is obtained for a modulus change of 1.72%, the maximum observed, due to frequency dispersion between the third and fifth harmonics.

This error is a sharp function of τ_0 and a reduction in R by a factor of 3 reduces the error to below 0.02%, a figure comparable to the measurement error of the normalized frequencies for large damping. Consequently, we may conclude that for all except the absolue worst-case conditions, Equation A20 approximates our data over the frequency regions of interest to within experimental error.

This fact is made clear in Fig. A1 in which data are plotted for 246.5 K, our worst-case conditions (see Figs. 2 and 3). Here the circles and crosses represent, respectively, measured and corrected normalized frequencies plotted as a function of mode number squared. Employing no adjustable parameters the data are brought into a straight

line using the third overtone for the reference frequency as mentioned previously.

References

1. N. G. McCRUM, B. E. READ and G. WILLIAMS, "Anelastic and Dielectric Effects in Polymeric Solids" (Wiley, London, 1967).
2. D. S. MUZZEY, Jr, *Phys. Rev.* **36** (1930) 935.
3. V. E. GIEBE and E. BLECHSCHMIDT, *Ann. Phys.* **5** (1933) 417, 457.
4. R. K. GALKIEWICZ and F. E. KARASZ, *J. Appl. Phys.* **49** (1978) 5233.
5. H. KOLSKY, "Stress Waves in Solids" (Dover Publications, New York, 1963) p. 41.
6. L. POCHHAMMER, *J. Reine Angew. Math.* **81** (1876) 324.
7. C. CHREE, *Q. J. Math.* **24** (1980) 340.
8. LORD RAYLEIGH, "The Theory of Sound", Vol. I (Dover Publications, New York, 1945) p. 251.
9. M. HORIO and S. ONOGI, *J. Appl. Phys.* **22** (1951) 977.
10. F. R. SCHWARZL and L. C. E. STRUIK, *Adv. Mol. Relax. Proc.* **1** (1967, 1968) 201.
11. G. NEMOZ, J. F. MAY and G. VALLET, *Rheol. Acta* **13** (1974) 66.
12. G. FARROW, J. McINTOSH and I. M. WARD, *Makromol. Chem.* **38** (1960) 147.
13. K. H. ILLERS and H. BREUER, *J. Colloid Sci.* **18** (1963) 1.
14. M. T. TAKEMORI, *Polymer Eng. Sci.* **18** (1978) 1193.
15. R. W. WARFIELD and F. R. BARNET, *Angew. Makromol. Chem.* **44** (1975) 181.
16. J. B. MARION, "Classical Dynamics of Particles and Systems" (Academic Press, New York, 1965) p. 141.

Received 11 June
and accepted 16 July 1982